Collisional model of quasilinear transport driven by toroidal electrostatic ion temperature gradient modes

I. Pusztai,[1] T. Fülöp,[1] J. Candy,[2] and R. J. Hastie[3]
[1]*Department of Radio and Space Science, Chalmers University of Technology, and Euratom-VR Association, SE-41296 Göteborg, Sweden*
[2]*General Atomics, P.O. Box 85608, San Diego, California 92186, USA*
[3]*EURATOM/UKAEA Fusion Association, Culham Science Centre, Abingdon, Oxon OX14 3DB, United Kingdom*

(Received 2 April 2009; accepted 15 June 2009; published online 13 July 2009)

The stability of ion temperature gradient (ITG) modes and the quasilinear fluxes driven by them are analyzed in weakly collisional tokamak plasmas using a semianalytical model based on an approximate solution of the gyrokinetic equation, where collisions are modeled by a Lorentz operator. Although the frequencies and growth rates of ITG modes far from threshold are only very weakly sensitive to the collisionality, the a/L_{Ti} threshold for stability is affected significantly by electron-ion collisions. The decrease in collisionality destabilizes the ITG mode driving an inward particle flux, which leads to the steepening of the density profile. Closed analytical expressions for the electron and ion density and temperature responses have been derived without expansion in the smallness of the magnetic drift frequencies. The results have been compared with gyrokinetic simulations with GYRO and illustrated by showing the scalings of the eigenvalues and quasilinear fluxes with collisionality, temperature scale length, and magnetic shear. © *2009 American Institute of Physics*. [DOI: 10.1063/1.3168611]

I. INTRODUCTION

Turbulent transport in tokamak plasmas is considered to be mainly caused by drift waves destabilized by trapped electrons and ion temperature gradients.[1–4] These microinstabilities and their effect on the transport can be studied by complex nonlinear gyrokinetic codes, for example GYRO.[5] To ease the interpretation of the results of these codes and experimental results it is useful to construct simpler models that can, after careful benchmarking with codes, give various parametric scalings. In particular, the collisionality dependence of the microinstabilities is interesting from both experimental and theoretical points of view. On the experimental side, the evolution of the density profile has been shown to depend on the collisionality.[6–10] On the theoretical side, it has been shown that the transport fluxes are dependent on the choice of the collision operator.[11]

Numerical simulations of ion temperature gradient (ITG) and trapped electron (TE) modes have shown that collisions may influence the sign and the magnitude of the quasilinear fluxes driven by these instabilities.[12] Without collisions, the quasilinear particle flux driven by ITG modes is usually inward due to curvature and thermodiffusion. Gyrokinetic calculations show that collisions drive an outward flux and the particle flux is expected to change sign for very small collisionalities, much smaller than the collisionality achievable in current tokamak experiments. The choice of the model collision operator affects the collisionality threshold for the reversal of the particle flux.[11] This means that collisionless models or models using the Krook model operator are not adequate to calculate the quasilinear transport fluxes for typical experimental parameters.

In this work we develop a collisional model for electrostatic turbulence (COMET) that can be used to analyze the stability of the ITG modes and to derive analytical expressions for the quasilinear fluxes. Much of the theoretical analysis of the effect of collisions on ITG modes has been based on an energy-dependent Krook operator.[13–15] Here, we model the collisions by a Lorentz operator, which automatically incorporates the increasing importance of pitch-angle scattering near the trapped-passing boundary.[16] We focus on weakly collisional plasmas with large aspect ratio and circular cross section and retain the effect of the magnetic drift nonperturbatively.

The collisionality dependence of the particle flux driven by microinstabilities has been studied in Ref. 11 under the assumption that the mode frequency and growth rate are independent of the collisionality. In this work, the model presented in Ref. 11 is extended to include the effect of collisions on the eigenfrequency, growth rate, and stability boundaries of the modes. We show that far from marginal stability the collisionality dependence of the ITG eigenfrequency and growth rate is weak and therefore will have a negligible effect on the particle fluxes. However, we found that the a/L_{Ti} stability threshold is sensitive to the electron-ion collisions. We found an exact ITG stability boundary in the adiabatic limit which incorporates the shear and the finite Larmor radius (FLR) parameter dependences.

To determine the perturbed electrostatic potential self-consistently would involve the solution of an integrodifferential equation that is analytically intractable. Therefore, as in Ref. 11, we use a model electrostatic potential, valid in the moderate shear region and motivated by a variational method. The model potential used here is improved compared to the one used in Ref. 11, by including a shear dependent imaginary part of the potential. Assuming this balloon-

ing model potential, closed analytical expressions for the electron and ion density and temperature perturbations are derived, without expansion in the smallness of the magnetic drift. These are used to compute the quasilinear particle and energy fluxes. The results of COMET are benchmarked with numerical gyrokinetic simulations with GYRO and are useful to show the scalings with collisionality, magnetic drift frequency, diamagnetic frequency, and ratio of the density and temperature scale lengths.

The remainder of the paper is organized as follows. In Sec. II, the perturbed electron and ion density and temperature responses are calculated. In Sec. III the dispersion relation is presented and the dependence of the stability boundaries on collisionality is studied. In Sec. IV the quasilinear transport fluxes are calculated and scalings of the growth rates, eigenfrequencies, and fluxes with temperature scale length, collisionality, and magnetic shear is discussed and compared with gyrokinetic simulations with GYRO. Finally, the results are summarized in Sec. V.

II. PERTURBED ELECTRON AND ION RESPONSES

The perturbed electron and ion responses are obtained from the linearized gyrokinetic (GK) equation,[13]

$$\frac{v_\parallel}{qR}\frac{\partial g_a}{\partial \theta} - i(\omega-\omega_{Da})g_a - C_a(g_a) = -i\frac{e_a f_{a0}}{T_a}(\omega-\omega_{*a}^T)\phi J_0(z_a), \tag{1}$$

where g_a is the nonadiabatic part of the perturbed distribution function, θ is the extended poloidal angle, ϕ is the perturbed electrostatic potential, $f_{a0}=n_a/(\sqrt{\pi}v_{Ta})^3\exp(-x_a^2)$ is the equilibrium Maxwellian distribution function, $x_a=v/v_{Ta}$ is the velocity normalized to the thermal speed $v_{Ta}=(2T_a/m_a)^{1/2}$, n_a, T_a, m_a, and e_a are the density, temperature, mass, and charge of species a, $\omega_{*a}=-k_\theta T_a/e_aBL_{na}$ is the diamagnetic frequency, $\omega_{*a}^T=\omega_{*a}\{1+[x_a^2-(3/2)]\eta_a\}$, $\eta_a=L_{na}/L_{Ta}$, $L_{na}=-[\partial(\ln n_a)/\partial r]^{-1}$, $L_{Ta}=-[\partial(\ln T_a)/\partial r]^{-1}$, are the density and temperature scale lengths, k_θ is the poloidal wave number, $\omega_{Da}=-k_\theta(v_\perp^2/2+v_\parallel^2)(\cos\theta+s\theta\sin\theta)/\omega_{ca}R$ is the magnetic drift frequency, $\omega_{ca}=e_aB/m_a$ is the cyclotron frequency, B is the equilibrium magnetic field, q is the safety factor, $s=(r/q)(dq/dr)$ is the magnetic shear, r and R are the minor and major radii, J_0 is the Bessel function of order zero, and $z_a=k_\perp v_\perp/\omega_{ca}$. We consider an axisymmetric, large aspect ratio torus with circular magnetic surfaces. We adopt the usual ordering for the relation of the electron/ion bounce frequencies and the eigenfrequency of the mode $\omega_{bi}\ll\omega\ll\omega_{be}$ and we consider weakly collisional plasmas so that $\nu_{\star e}=\nu_e/\epsilon\omega_{be}\ll 1$, where ν_e is the electron-ion collision frequency and $\epsilon=r/R$ is the inverse aspect ratio. The ion self-collisions and ion-electron collisions are neglected $[C_i(g_i)=0]$, while the electron-ion collisions are modeled by a pitch-angle scattering operator

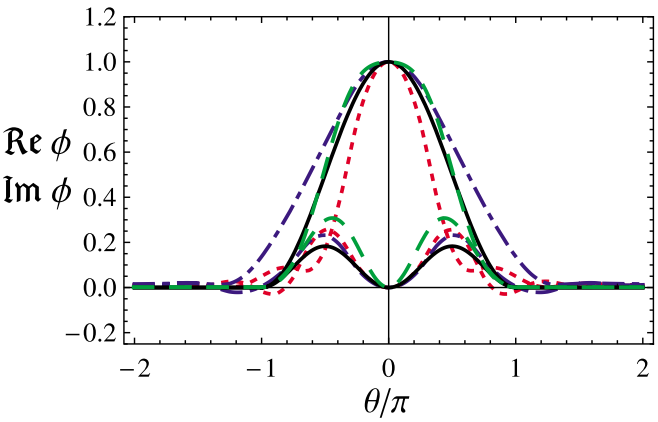

FIG. 1. (Color online) Electrostatic potential as a function of ballooning angle. Solid black line is the potential used in COMET, green dashed line is the potential calculated by a variational approach in Appendix A, red dotted line is the linear GYRO-result without parallel ion motion and blue dash-dotted line is the linear GYRO-result with parallel ion motion. The lower curves are the imaginary part of the potential. The parameters are $\eta_e=\eta_i=3$, $s=1$, $q=2$, $\epsilon=1/6$, and $L_n/R=1/3$.

$$C_e = \nu_e(v)\frac{2\xi}{B}\frac{\partial}{\partial\lambda}\xi\lambda\frac{\partial}{\partial\lambda} \equiv \nu_e(v)\mathcal{L}, \tag{2}$$

where $\nu_e(v)=\nu_T/x_e^3$, ν_T is the electron-ion collision frequency at the thermal speed, $\xi=v_\parallel/v$, $\lambda=2\mu/(m_ev^2)$, and $\mu=m_ev_\perp^2/2B$.

Experience from GYRO simulations leads us to adopt the following form for the perturbed electrostatic potential:

$$\phi(\theta)=\phi_0\left(\frac{1+\cos\theta}{2}+if_s\sin^2\theta\right)[H(\theta+\pi)-H(\theta-\pi)], \tag{3}$$

where H is the Heaviside function. The coefficient f_s in front of the imaginary part depends on the plasma parameters, e.g., shear, safety factor, density, and temperature gradients. Gyrokinetic simulations with GYRO show that the shear dependence of f_s is the most important factor and f_s can approximately be written as $f_s=-0.6s+s^2-0.3s^3$. We outline a motivation for the chosen model in Appendix A, where we construct an approximation for the perturbed electrostatic potential in the collisionless limit by a variational method using a trial function similar to the one assumed in Eq. (3). Figure 1 shows that the model electrostatic potential from Eq. (3) is in good agreement with the numerical solution for the potential given by GYRO and the variationally calculated potential calculated in Appendix A. The approximation for the perturbed electrostatic potential breaks down for low and high shear (outside the region $0.2<s<1.7$) or near marginal instability, but as we will show, the qualitative features of the transport are captured by our calculations, although for quantitatively accurate results one of course has to resort to numerical simulations.

A. Electron response

The circulating electrons are assumed to be adiabatic. The nonadiabatic electron distribution can be expanded $g_e=g_{e0}+g_{e1}+\cdots$ in the smallness of ω/ω_{be} and the normal-

ized collisionality $\nu_{\star e}$, which gives $\partial g_{e0}/\partial\theta=0$ in lowest order. The electron GK equation is orbit averaged between the mirror reflection points providing a constraint for g_{e0},

$$i(\omega-\langle\omega_{De}\rangle)g_{e0}+\langle C_e(g_{e0})\rangle=(ie\langle\phi\rangle/T_e)(\omega_{*e}^T-\omega)f_{e0}, \quad (4)$$

where $\langle\cdots\rangle$ is an average over the bounce-orbit of the trapped electrons. Using WKB-analysis to solve the homogeneous equation and then the method of variation of parameters to determine the solution of the inhomogeneous equation it is possible to construct an approximate solution to the orbit averaged GK equation.[11] The homogeneous solution of the electron gyrokinetic equation, obtained by WKB-analysis for weakly collisional plasmas, $\hat{\nu}\equiv\nu_e/\omega_0\epsilon\ll1$, is

$$g_{\rm hom}(\kappa)=\frac{1}{(\kappa u)^{1/4}}(c_1\sinh z^2+c_2\cosh z^2), \quad (5)$$

where $z=\sqrt{2}(\kappa u/\hat{\nu})^{1/4}$ and $\kappa=[1-\lambda B_0(1-\epsilon)]/(2\epsilon\lambda B_0)$. In addition, B_0 is the flux-surface averaged magnetic field, $\omega_0=\omega/y$ is the absolute value of the real part of the eigenfrequency, $y=\sigma+i\hat{\gamma}$, $\sigma=\text{sign}(\Re\{\omega\})$, $\hat{\gamma}$ is the growth rate normalized to ω_0, $u=-iy(2-\tilde{\omega}_D)$, and $\tilde{\omega}_D=\omega_{D0}/\omega$ with $\omega_{D0}=-k_\theta v^2/\omega_{ce}R$ is the normalized magnetic drift frequency. In the limit $z\to\infty$ (consistent with the assumption $\hat{\nu}\ll1$), the inhomogeneous part of the distribution can be simplified to

$$g_{\rm inhom}(\kappa)=\frac{\hat{S}}{2\omega(2-\tilde{\omega}_D)}(4-\sqrt{\pi}e^{z^2}/z), \quad (6)$$

where $\hat{S}=-(e\phi_0/T_e)(8/3\pi)(1+i4f_s/5)(\omega-\omega_{*e}^T)f_{e0}$. In these expressions, we expressed the bounce average of the potential as

$$\langle\phi\rangle=\phi_0\left\{\frac{E(\kappa)}{K(\kappa)}+i\frac{4f_s}{3}\left[(2\kappa-1)\frac{E(\kappa)}{K(\kappa)}+1-\kappa\right]\right\},$$

where $E(\kappa)$ and $K(\kappa)$ are complete elliptic integrals. To obtain Eqs. (5) and (6) we approximated the elliptic integrals with their asymptotic limits for small arguments. Since $g_{e0}(\kappa=0)$ is regular, we choose $c_2=0$, and the boundary condition $g_{e0}(\kappa=1)=0$[16,17] gives $c_1=-g_{\rm inhom}(1)u^{1/4}/\sinh(2\sqrt{u/\hat{\nu}})$ so that the solution for the perturbed trapped-electron distribution is

$$g_{e0}=\frac{\hat{S}(4-\sqrt{\pi}e^{z^2}/z)}{2\omega(2-\tilde{\omega}_D)}-\frac{\hat{S}(4-\sqrt{\pi}e^{z^2/\sqrt{\kappa}}\kappa^{1/4}/z)}{2\kappa^{1/4}\omega(2-\tilde{\omega}_D)}\frac{\sinh(z^2)}{\sinh(z^2/\sqrt{\kappa})}, \quad (7)$$

except in a narrow layer close to $\kappa=0$ that has a negligible contribution to the velocity space integrals.

The perturbed electron response is proportional to

$$\left\langle\int g_{e0}d^3v\right\rangle=4\sqrt{2\epsilon}\int_0^\infty v^2dv\int_0^1K(\kappa)g_{e0}d\kappa=\frac{16\sqrt{2\epsilon}}{\omega}\int_0^\infty\frac{v^2dv\hat{S}}{(2-\tilde{\omega}_D)}\left(1-\sqrt{\frac{\hat{\nu}}{u}}\right), \quad (8)$$

where we retained terms only to the lowest order in $\hat{\nu}^{1/2}$ and approximated $\int_0^1K(\kappa)g_{e0}d\kappa\simeq2\int_0^1g_{e0}d\kappa$. The expression in Eq. (8) has been compared with a numerical solution to the electron GK equation resulting in excellent agreement for $\hat{\nu}$ up to $O(1)$ values. The velocity integral in Eq. (8) can be evaluated in terms of ${}_2F_0$ generalized hypergeometric functions[18] and the perturbed electron density response becomes

$$\frac{\hat{n}_e}{n_e}\Big/\frac{e\phi}{T_e}=1-\tilde{\phi}\left\{\sqrt{2\epsilon}\left[\hat{\omega}_{\eta^*e}-\frac{3}{2}\left(\eta_e\tilde{\omega}_{*e}-\frac{\tilde{\omega}_{Dt}}{2}\hat{\omega}_{\eta^*e}\right)\times\mathcal{F}^1_{5/2}\left(\frac{\tilde{\omega}_{Dt}}{2}\right)\right]-\frac{\Gamma\left(\frac{3}{4}\right)\sqrt{\epsilon\hat{\nu}_t}}{\sqrt{-i\pi y}}\times\left[2\hat{\omega}_{\eta^*e}\mathcal{F}^{3/2}_{3/4}\left(\frac{\tilde{\omega}_{Dt}}{2}\right)-\frac{3\eta_e\tilde{\omega}_{*e}}{2}\mathcal{F}^{3/2}_{7/4}\left(\frac{\tilde{\omega}_{Dt}}{2}\right)\right]\right\}, \quad (9)$$

where $\tilde{\phi}=(1+4if_s/5)16\phi_0/(3\pi^2\phi)$, $\mathcal{F}^a_b(z)={}_2F_0(a,b;;z)$, $\tilde{\omega}_{Dt}=\omega_{D0}/(\omega x_e^2)$, $\hat{\nu}_t=\hat{\nu}x_e^3$, $\tilde{\omega}_{*e}=\omega_{*e}/\omega$, and $\hat{\omega}_{\eta^*a}=1-(1-3\eta_a/2)\tilde{\omega}_{*a}$. The perturbed electron temperature can be derived from the nonadiabatic electron distribution function given in Eq. (7) to be

$$\frac{\hat{T}_e}{T_e}\Big/\frac{e\phi}{T_e}=\frac{3\tilde{\phi}}{2}\left\{-\sqrt{2\epsilon}\left[\hat{\omega}_{\eta^*e}-\frac{5}{2}\left(\eta_e\tilde{\omega}_{*e}-\frac{\tilde{\omega}_{Dt}}{2}\hat{\omega}_{\eta^*e}\right)\times\mathcal{F}^1_{7/2}\left(\frac{\tilde{\omega}_{Dt}}{2}\right)\right]+\frac{\Gamma\left(\frac{3}{4}\right)\sqrt{\epsilon\hat{\nu}_t}}{\sqrt{-i\pi y}}\times\left[\hat{\omega}_{\eta^*e}\mathcal{F}^{3/2}_{7/4}\left(\frac{\tilde{\omega}_{Dt}}{2}\right)-\frac{7\eta_e\tilde{\omega}_{*e}}{4}\mathcal{F}^{3/2}_{11/4}\left(\frac{\tilde{\omega}_{Dt}}{2}\right)\right]\right\}. \quad (10)$$

The hypergeometric functions appearing in the perturbed electron and ion responses can be approximated by a simple algebraic expression $\mathcal{F}^{a_1}_{a_2}(z)\approx(1-\sqrt{b+\sqrt{b-z}})^{-c}$, where the coefficients c and b are given in Appendix B.

B. Ion response

For the ions we neglect the parallel dynamics by assuming $k_\parallel v_{Ti}\ll\omega$. In this limit Eq. (1) can be solved by neglecting the parallel derivative and replacing ω_{Di} with its weighted flux-surface averaged value $\langle\omega_{Di}\rangle_\phi$, where $\langle X(\theta)\rangle_\phi=\int_{-\pi}^{\pi}X(\theta)\phi(\theta)d\theta/\int_{-\pi}^{\pi}\phi(\theta)d\theta$. The perturbed ion response becomes

$$\frac{\hat{n}_i}{n_i}=\frac{e\phi}{T_i}\left[-1+\int d^3v\frac{f_{i0}J_0^2(z_i)(1-\omega_{*i}^T/\omega)}{1-x_i^2\tilde{\omega}_{Ds}}\right]\equiv\frac{e\phi(-1+I_v)}{T_i}, \quad (11)$$

where

$$\tilde{\omega}_{Ds}=\frac{6+(9+16if_s)s}{12(1+if_s)}\frac{\omega_{Di0}}{\omega},$$

$\omega_{Di0}=-2k_\theta v_{Ti}^2/3\omega_{ci}R$ and we used the constant energy resonance (CER) approximation for the ion resonance $[v_\perp^2+2v_\parallel^2\to4(v_\perp^2+v_\parallel^2)/3]$.[13]

The nonadiabatic part of the ion response can be obtained by the evaluation of the velocity integral of Eq. (11),

$$I_v = \frac{2}{\sqrt{\pi}}\int_0^\infty dx_\perp x_\perp \int_{-\infty}^\infty dx_\parallel e^{-x^2} J_0^2(x_\perp\sqrt{2b_s}) \times \frac{1-[1-(x^2-3/2)\eta_i]\tilde{\omega}_{*i}}{1-x^2\tilde{\omega}_{Ds}}, \quad (12)$$

where we introduced the FLR-parameter $b_s=b_0(1+s^2\theta^2)$ with $b_0=(k_\theta\rho_i)^2$. Also, $\rho_i=c_s/(\sqrt{\tau}\omega_{ci})$ is the ion sound Larmor radius, $\tau=T_e/T_i$ is the electron-to-ion temperature ratio, and $c_s=\sqrt{T_e/m_i}$ is the ion sound speed. In order to make further progress analytically, we restrict our analysis to long wavelength perturbations and keep only the linear terms in b_0. This approximation is typically valid for the fastest growing ITG modes ($k_\theta\rho_i\sim 0.2$). Then I_v can be evaluated to obtain the perturbed ion response

$$\frac{\hat{n}_i}{n_i}\Big/\frac{e\phi}{T_i} = -\tilde{\omega}_{*i} + \left(\frac{3\tilde{\omega}_{Ds}}{2}-b\right) \times\left[\hat{\omega}_{\eta^*i} - \frac{5}{2}(\eta_i\tilde{\omega}_{*i}-\tilde{\omega}_{Ds}\hat{\omega}_{\eta^*i})\mathcal{F}^1_{7/2}(\tilde{\omega}_{Ds})\right], \quad (13)$$

where $b=\langle b_s\rangle_\phi = b_0\{1+s^2[2\pi^2-12+if_s(2\pi^2-3)]/[6(1+if_s)]\}$ is the weighted flux-surface averaged value of the FLR parameter. Note that the expressions for the perturbed electron and ion density in Eqs. (9) and (13) are exact in ω_{Da}; no approximation regarding the relative magnitude of ω_{Da} and ω has been made. Evaluating an integral similar to Eq. (12) but with the integrand multiplied by x^2 leads to the nonadiabatic perturbed ion temperature response,

$$\frac{\hat{T}_i}{T_i}\Big/\frac{e\phi}{T_i} = \frac{3}{2}[1-(1+\eta_i)\tilde{\omega}_{*i}] + \frac{5}{2}\left(\frac{3\tilde{\omega}_{Ds}}{2}-b\right) \times\left[\hat{\omega}_{\eta^*i} - \frac{7}{2}(\eta_i\tilde{\omega}_{*i}-\tilde{\omega}_{Ds}\hat{\omega}_{\eta^*i})\mathcal{F}^1_{9/2}(\tilde{\omega}_{Ds})\right]. \quad (14)$$

C. Nonresonant expansion

In the limit of low normalized magnetic drift frequencies, expanding Eq. (9) around $\tilde{\omega}_{Dt}=0$ and keeping only the first order terms (usually called the nonresonant expansion), the perturbed electron density reduces to the following expression:

$$\frac{\hat{n}_e}{n_e}\Big/\frac{e\phi}{T_e} = 1-\tilde{\phi}\left\{\sqrt{2\epsilon}\left\{(1-\tilde{\omega}_{*e})+\frac{3\tilde{\omega}_{Dt}}{4}[1-(1+\eta_e)\tilde{\omega}_{*e}]\right\} - \frac{2\Gamma\left(\frac{3}{4}\right)i\sqrt{-iy\epsilon\hat{\nu}_t}}{\sqrt{\pi}y}\left\{1-\left(1-\frac{3\eta_e}{4}\right)\tilde{\omega}_{*e} + \frac{9\tilde{\omega}_{Dt}}{16}\left[1-\left(1+\frac{\eta_e}{4}\right)\tilde{\omega}_{*e}\right]\right\}\right\}. \quad (15)$$

For the ions, expanding Eq. (13) in $\tilde{\omega}_{Ds}$ leads to

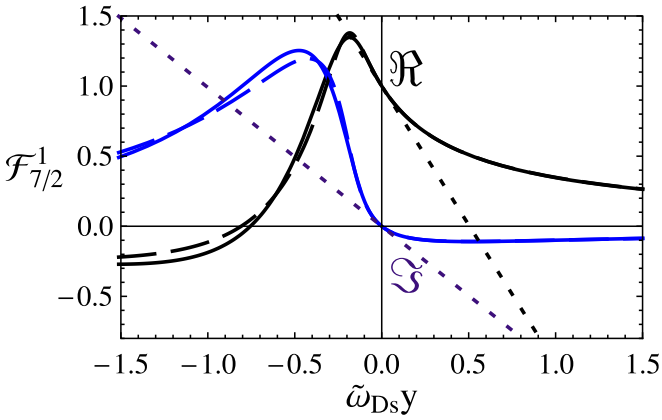

FIG. 2. (Color online) $\mathcal{F}^1_{7/2}(\tilde{\omega}_{Ds})$ for $y=-1+0.5i$. Solid lines: exact. Dotted lines: expansion around $\tilde{\omega}_{Ds}=0$. Dashed lines: approximation discussed in Appendix B, Eq. (B1).

$$\frac{\hat{n}_i}{n_i}\Big/\frac{e\phi}{T_i} = -b-[1-b(1+\eta_i)]\tilde{\omega}_{*i} + \{(3-5b)-[3(1+\eta_i)-5b(1+2\eta_i)]\tilde{\omega}_{*i}\}\frac{\tilde{\omega}_{Ds}}{2}. \quad (16)$$

However, as we will show, the results based on the expansions in $\tilde{\omega}_{Dt}$ and $\tilde{\omega}_{Ds}$ in Eqs. (15) and (16), respectively, will give large errors compared to the exact solutions in Eqs. (9) and (13). The inability of the nonresonant expansion to reproduce the correct eigenvalues and fluxes has been noted before in Ref. 12. The reason for this is illustrated in Fig. 2 where the difference between the exact and an expanded solution is shown for one of the hypergeometric functions. The solid lines correspond to the real (black) and imaginary (blue) parts of the generalized hypergeometric function appearing in the ion response [Eq. (13)], their expansion to first order around $\tilde{\omega}_{Ds}=0$ are plotted with dotted lines, while the dashed lines correspond to a simple algebraic approximation discussed in Appendix B. The ITG mode with $\hat{\gamma}=0.5$, $\omega_r=-\omega_{*e}$ for $R/L_n=3$, $s=1$ would correspond to $\tilde{\omega}_{Ds}y\simeq 0.84$.

D. Summary of analytical formulas

Using the approximative formula for the hypergeometric functions from Appendix B, the perturbed electron density, and temperature responses, $\bar{n}_a=\hat{n}_aT_a/(n_ae\phi)$ and $\bar{T}_a=\hat{T}_a/e\phi$ can be written as

$$\bar{n}_e = 1-\tilde{\phi}\left\{\sqrt{2\epsilon}\left[\hat{\omega}_{\eta^*e}-\frac{3}{2}\frac{(\eta_e\tilde{\omega}_{*e}-\tilde{\omega}_{Dt}\hat{\omega}_{\eta^*e}/2)}{[3/5+\sqrt{(2/5)^2-\tilde{\omega}_{Dt}/2}]^2}\right] - \frac{\Gamma\left(\frac{3}{4}\right)\sqrt{\epsilon\hat{\nu}_t}}{\sqrt{-i\pi y}}\left[\frac{2\hat{\omega}_{\eta^*e}}{[4/9+\sqrt{(5/9)^2-\tilde{\omega}_{Dt}/2}]^{5/4}} - \frac{3\eta_e\tilde{\omega}_{*e}}{2[11/21+\sqrt{(10/21)^2-\tilde{\omega}_{Dt}/2}]^{5/2}}\right]\right\}, \quad (17)$$

$$\bar{T}_e = \frac{3\tilde{\phi}}{2}\left\{ -\sqrt{2\epsilon}\left[\hat{\omega}_{\eta^* e} - \frac{5(\eta_e\tilde{\omega}_{*e} - \tilde{\omega}_{Dt}\hat{\omega}_{\eta^* e}/2)}{2[9/14 + \sqrt{(5/14)^2 - \tilde{\omega}_{Dt}/2}]^{5/2}} \right] + \frac{\Gamma\left(\frac{3}{4}\right)\sqrt{\epsilon\hat{\nu}_t}}{\sqrt{-i\pi y}}\left[\frac{\hat{\omega}_{\eta^* e}}{[11/21 + \sqrt{(10/21)^2 - \tilde{\omega}_{Dt}/2}]^{5/2}} - \frac{7\eta_e\tilde{\omega}_{*e}}{4[7/11 + \sqrt{(4/11)^2 - \tilde{\omega}_{Dt}/2}]^3} \right] \right\}. \quad (18)$$

The perturbed ion density and temperature responses are

$$\bar{n}_i = -\tilde{\omega}_{*i} + \left(\frac{3\tilde{\omega}_{Ds}}{2} - b\right) \times \left[\hat{\omega}_{\eta^* i} - \frac{5(\eta_i\tilde{\omega}_{*i} - \tilde{\omega}_{Ds}\hat{\omega}_{\eta^* i})}{2[9/14 + \sqrt{(5/14)^2 - \tilde{\omega}_{Ds}}]^{5/2}} \right], \quad (19)$$

$$\bar{T}_i = \frac{3}{2}[1 - (1+\eta_i)\tilde{\omega}_{*i}] + \frac{5}{2}\left(\frac{3\tilde{\omega}_{Ds}}{2} - b\right) \times \left[\hat{\omega}_{\eta^* i} - \frac{7(\eta_i\tilde{\omega}_{*i} - \tilde{\omega}_{Ds}\hat{\omega}_{\eta^* i})}{2(2/3 + \sqrt{1/9 - \tilde{\omega}_{Ds}})^3} \right]. \quad (20)$$

The formulas, which we summarized above, are the most accurate known for moderate magnetic shear and they can be used to compute the dispersion relation and the quasilinear fluxes as shown in the following chapters. They are useful in showing the scalings with collisionality, magnetic drift frequency, diamagnetic frequency and ratio of the density and temperature scale lengths.

III. STABILITY

The dispersion relation follows from the quasineutrality condition $\hat{n}_i = \hat{n}_e$, where the perturbed electron and ion densities are given by Eqs. (9) and (13), respectively, and we take a flux-surface average. The dispersion relation obtained here is valid for both ITG propagating in the ion diamagnetic direction ($\sigma=-1$) and TE modes propagating in the electron diamagnetic direction ($\sigma=1$), but in this paper, we will focus only on the ITG mode stability and the quasilinear fluxes driven by them. The effect of collisions modeled by a Lorentz operator on the stability of TE modes has been studied before in the steep density and temperature gradient region,[17] where the curvature drift can be neglected.

In the limit of large aspect ratio, $\epsilon \to 0$, the trapped part of the perturbed electron density can be neglected and the dispersion relation reduces to the following expression for ITG ($\sigma=-1$) modes with adiabatic electrons:

$$1 = \tau\left\{ -\tilde{\omega}_{*i} + \left(\frac{3\tilde{\omega}_{Ds}}{2} - b\right) \times \left[\hat{\omega}_{\eta^* i} - \frac{5}{2}(\eta_i\tilde{\omega}_{*i} - \tilde{\omega}_{Ds}\hat{\omega}_{\eta^* i})\mathcal{F}^1_{7/2}(\tilde{\omega}_{Ds}) \right] \right\}. \quad (21)$$

Using the condition of marginal instability $\gamma=0$, we can derive an approximate stability condition for the ITG modes. We start by noting that the imaginary part of $\tilde{\omega}_{Ds}$ is negligible if $(7s-6)f_s/(6+9s+16f_s^2 s) \ll 1$ and the imaginary part of b is also negligible when $9f_s s^2/[2(3+(\pi^2-6)s^2)] \ll 1$ and $f_s^2 \ll 1$, in which case the expression in Eq. (21) is real except for the term containing the function $\mathcal{F}^2_{7/2}(\tilde{\omega}_{Ds})$ that has an imaginary part for all values except $\tilde{\omega}_{Ds}=0$. Therefore, the condition $\gamma=0$ can only be satisfied if the coefficient of $\mathcal{F}^2_{7/2}(\tilde{\omega}_{Ds})$ vanishes. Using $\tilde{\omega}_{*i} = -\tilde{\omega}_{*e}/\tau$ and $\omega_{Di0} = -2\omega_{*e}\epsilon_n/\tau$, where $\epsilon_n = L_n/R$, the ω_0 for which the coefficient of $\mathcal{F}^2_{7/2}(\tilde{\omega}_{Ds})$ is zero can be shown to be

$$\omega_0 = \frac{(2+3s)(3\eta_i - 2)\epsilon_n\omega_{*e}}{2\tau[(2+3s)\epsilon_n - 3\eta_i]}, \quad (22)$$

where we set $\sigma=-1$ for ITG modes. The critical η_i for stability satisfies the remaining part of Eq. (21),

$$\frac{1}{\tau} = \left(\frac{3\tilde{\omega}_{Ds}}{2} - b\right)\hat{\omega}_{\eta^* i} - \tilde{\omega}_{*i}. \quad (23)$$

Equation (23) can be rewritten as $3(b-1)\eta_i\tau + (2+3s)(1+\tau)\epsilon_n = 0$, so that the ITG stability boundary for adiabatic electrons becomes

$$\eta_{ic} = \left(1 + \frac{1}{\tau}\right)\frac{(2+3s)\epsilon_n}{3(1-b)}, \quad (24)$$

and the corresponding critical real frequency of the mode is

$$\frac{\omega_{0c}}{\omega_{*e}} = \frac{b-1}{\tau b + 1} + \left(1 + \frac{1}{\tau}\right)\frac{(2+3s)\epsilon_n}{(\tau b+1)2}. \quad (25)$$

For $b=0$ and $s=1$, the critical η_i given in Eq. (24) is similar to what was found previously in the local kinetic limit:[13] $\eta_{ic} = 4(1+1/\tau)\epsilon_n/3$. In the present model the coefficient of $(1+1/\tau)\epsilon_n$ is 5/3 for $s=1$, because the flux surface average of the magnetic drift frequency was used instead of its value at $\theta=0$ as in Ref. 13.

If we retain the trapped electron contribution, in the limit of low collisionality $\nu_e/(\omega_0\epsilon) \ll 1$ the dispersion relation becomes

$$\tau\left\{ -\tilde{\omega}_{*i} + \left(\frac{3\tilde{\omega}_{Ds}}{2} - b\right)\left[\hat{\omega}_{\eta^* i} - \frac{5}{2}(\eta_i\tilde{\omega}_{*i} - \tilde{\omega}_{Ds}\hat{\omega}_{\eta^* i})\mathcal{F}^1_{7/2}(\tilde{\omega}_{Ds}) \right] \right\} = 1 - \frac{(1+4if_s/5)32}{(1+if_s)3\pi^2}\left\{ \sqrt{2\epsilon}\left[\hat{\omega}_{\eta^* e} - \frac{3}{2}\left(\eta_e\tilde{\omega}_{*e} - \frac{\tilde{\omega}_{Dt}}{2}\hat{\omega}_{\eta^* e}\right)\mathcal{F}^1_{5/2}\left(\frac{\tilde{\omega}_{Dt}}{2}\right) \right] - \frac{\Gamma\left(\frac{3}{4}\right)\sqrt{\epsilon\hat{\nu}_t}}{\sqrt{-i\pi y}}\left[2\hat{\omega}_{\eta^* e}\mathcal{F}^{3/2}_{3/4}\left(\frac{\tilde{\omega}_{Dt}}{2}\right) - \frac{3\eta\tilde{\omega}_{*e}}{2}\mathcal{F}^{3/2}_{7/4}\left(\frac{\tilde{\omega}_{Dt}}{2}\right) \right] \right\}. \quad (26)$$

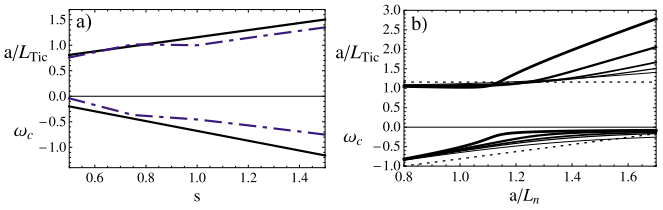

FIG. 3. (Color online) Stability boundaries of the ITG mode. The upper curves are the critical a/L_{Ti} and the lower ones are the real frequency of the mode normalized to $k_\theta \rho_i c/a$. The parameters are $\eta_e=3$, $q=2$, and $\epsilon=1/6$. Left: shear scaling of the stability boundary and real frequency for $a/L_n=1$. The solid black lines are from COMET for adiabatic electrons and the dash-dotted blue lines are the results of linear GYRO simulations. Right: a/L_n-scaling of the stability boundary and real frequency for $s=1$. The collisionality increases from the thin to the thick lines: $\nu_T/(\epsilon k_\theta \rho_i c/a)=0, 0.0125, 0.025, 0.05, 0.1$. The stability boundary for adiabatic electrons is indicated with dotted lines.

Figure 3(a) shows the stability boundaries and real frequencies of the ITG-mode as a function of shear, together with linear GYRO simulations in the collisionless case. The results of COMET are in satisfactory agreement with the results of linear GYRO simulations. Very good agreement with GYRO has been found also in b, τ, and ϵ_n scalings. Figure 3(b) shows the stability boundaries and real frequencies of the ITG mode in the $a/L_{Ti}-a/L_n$ space for various collisionalities. Clearly, the stability boundaries are significantly affected by the collisionality. The collisionality increases from thin to thick lines and already a small amount of collisionality affects the a/L_{Ti} threshold for high enough a/L_n. This means that if we decrease the collisionality, for a constant temperature gradient, much higher density gradient is needed for the stabilization of the ITG mode.

IV. QUASILINEAR FLUXES

The collisionality dependence of the quasilinear particle fluxes has been studied previously in Ref. 11, but without solving the dispersion relation, and neglecting the effect of the collisionality on these quantities. Here we study the dependence of the transport fluxes including the effect of collisions on the eigenfrequency and we benchmark the results with linear calculations with GYRO. The quasilinear particle flux is ambipolar and is given by

$$\Gamma_e = -\frac{k_\theta p_e}{eB}\left|\frac{e\bar{\phi}}{T_e}\right|^2 \Im\left(\frac{\bar{\hat{n}}_e/n_e}{e\bar{\phi}/T_e}\right), \tag{27}$$

where the overbar denotes the flux-surface average of the perturbed quantities and $\bar{\phi}=\phi_0(1+if_s)/2$. The quasilinear energy flux for particle species a is defined by

$$Q_a = -\frac{k_\theta p_a T_a}{eB}\left|\frac{e\bar{\phi}}{T_a}\right|^2 \Im\left(\frac{\bar{\hat{T}}_a/T_a}{e\bar{\phi}/T_a}\right). \tag{28}$$

The quasilinear fluxes can be evaluated using the expressions for the perturbed electron and ion density and temperature responses given in Sec. II in Eqs. (9), (11), and (14). Quite accurate approximate results can be obtained also from the formulas listed in Sec. II C, Eqs. (17), (19), and (20), respectively.

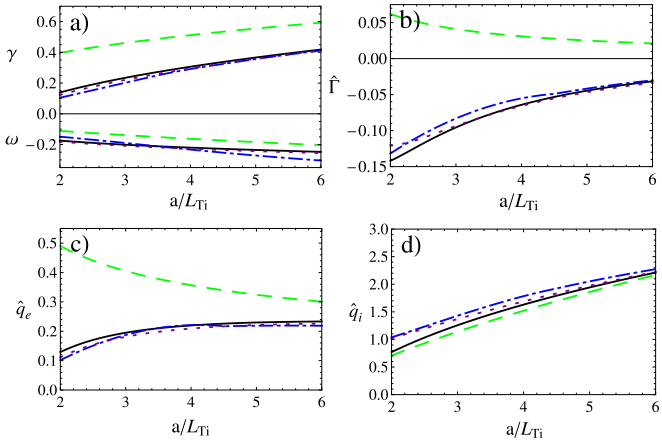

FIG. 4. (Color online) a/L_{Ti} scans of the eigenfrequency, growth rate (normalized to c_s/a), particle flux, and ion and electron energy fluxes (normalized to $k_\theta p_e/eB|e\bar{\phi}/T_e|^2$ and $k_\theta p_a T_a/eB|e\bar{\phi}/T_a|^2$, respectively). Black solid line is COMET, purple dotted line is with the algebraic approximation to the hypergeometric functions, blue dash-dotted line is the quasilinear GYRO result with ion parallel motion, and green dashed line is the result of the nonresonant expansion. The red dots correspond to nonlinear GYRO simulations.

In the following we will present the a/L_{Ti}, collisionality, and shear scalings of the eigenfrequency, growth rate, particle flux and electron and ion energy fluxes, together with quasilinear and nonlinear GYRO results for the following parameter set $a/L_{Te}=a/L_{Ti}=3$, $s=1$, $q=2$, $a/R=1/3$, $a/R=2$, and $a/L_n=1$ (i.e., the GA standard case[5]). Each GYRO nonlinear simulation used a perpendicular domain size of $(L_x/\rho_i, L_y/\rho_i)=(86, 90)$, fully resolving modes with wave numbers in the range $k_x\rho_i \leq 2.3$ and $k_y\rho_i \leq 1.1$. The standard 128-point velocity-space grid (eight energies, eight pitch angles, and two signs of velocity) was used. Electrons were taken to be drift kinetic with $\sqrt{m_i/m_e}=60$ and the simplified $s-\alpha$ geometry equilibrium model was used.

A. a/L_{Ti}-scaling

Figure 4 shows the a/L_{Ti} scalings of the eigenvalues and the fluxes in the collisionless case. The COMET results (solid line) are compared with quasilinear GYRO (blue dash-dotted line) and nonlinear GYRO (red dots) simulation results. For comparison, the results computed by expanding to first order in ω_D/ω (nonresonant expansion) are shown with green dashed lines and the results using the algebraic approximations to the hypergeometric functions are shown with purple dotted lines. The frequencies are normalized to c_s/a, where a is the minor radius, while the particle and energy fluxes are normalized to $k_\theta p_e/eB|e\bar{\phi}/T_e|^2$ and $k_\theta p_a T_a/eB|e\bar{\phi}/T_a|^2$, respectively. The comparisons to the nonlinear simulations are based on the choice of the flux surface averaged perturbed potential amplitude $\bar{\phi}$ so that $|e\bar{\phi}/T_e|/\rho_*=6.5$, where $\rho_*=\rho_i/a$, which is consistent with the usual mixing length estimate $\hat{n}_e/n_e \sim 1/(k_\theta L_n)$. The agreement between COMET and quasilinear GYRO results is very good. The disagreement with the nonresonant expansion (green dashed line) is large, but not surprising, since $\omega_D \sim \omega$.

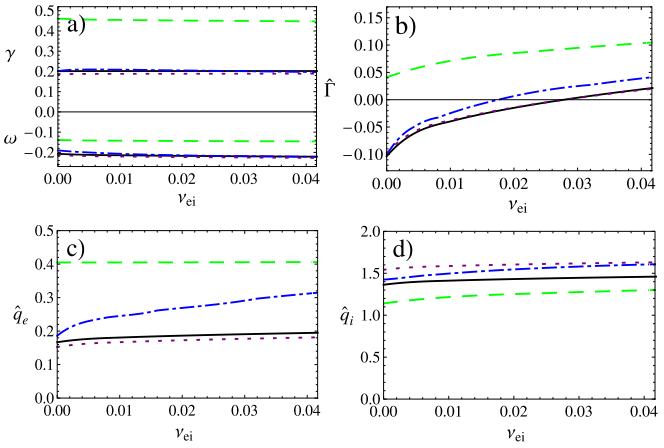

FIG. 5. (Color online) Collisionality scans of the eigenfrequency, growth rate, particle flux, and ion and electron energy fluxes. Black solid line is COMET, purple dotted line is with the algebraic approximation to the hypergeometric functions, blue dash-dotted line is the quasilinear GYRO result with ion parallel motion, and green dashed line is the result of the nonresonant expansion. The red dots correspond to nonlinear GYRO simulations.

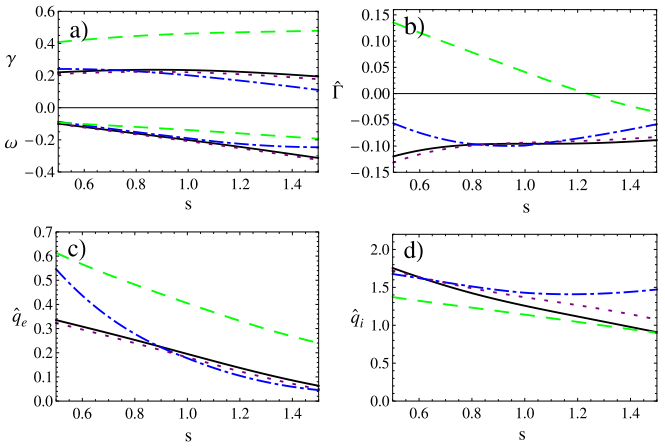

FIG. 6. (Color online) Shear scans of the eigenfrequency, growth rate, particle flux, and ion and electron energy fluxes. Black solid line is COMET, purple dotted line is with the algebraic approximation to the approximate hypergeometric functions, blue dash-dotted line is the quasilinear GYRO result with ion parallel motion, and green dashed line is the result of the nonresonant expansion.

The particle fluxes are inward and their absolute values decrease with a/L_{Ti}, but the electron and ion energy fluxes increase with a/L_{Ti}. The disagreement between the full COMET solution and the nonresonant expansion is remarkable for the particle flux, which shows that the nonresonant expansion fails to reproduce both the sign and the magnitude of the particle fluxes. Furthermore, the nonresonant expansion gives incorrect scaling for the electron energy flux as a function of η_i.

B. Collisionality scaling

Figure 5 shows the collisionality scaling of the eigenvalues and fluxes. As in Fig. 4 we show the COMET results compared to quasilinear and nonlinear GYRO results together with the nonresonant expansion. The collisionality ν_{ei} is defined in units of c_s/a and is $\nu_{ei} = (n_e e^4 \ln \Lambda)/[4\pi\epsilon_0^2(2T_e)^{3/2}\sqrt{m_e}]$, where $\ln \Lambda$ is the Coulomb logarithm. The results show that the eigenfrequency and growth rate of the ITG mode are insensitive to the collisionality, therefore the quasilinear particle flux driven by ITG is almost identical to the one calculated in Ref. 11, where the collisionality dependence of the eigenvalues was neglected. As noted before, the particle flux changes sign from inward to outward at a certain value of the collisionality. The electron and ion energy fluxes depend only weakly on collisions. Again, the agreement between COMET and GYRO results is very good. Also here, the nonresonant solution departs considerably from the full solution, both for the eigenvalues and the fluxes. As noted in previous work,[11] the Krook and Lorentz model operators lead to different results, although for cases far from marginal instability, as it is the case for the parameters used in this paper, they are in qualitative agreement.

The collisionality dependence of the electron heat flux differs from the quasilinear GYRO results. The COMET results exhibit almost no dependence on collisions but the quasilinear GYRO results show that collisions drive an outward electron heat flux. This is mainly due to the fact that the assumed ballooning potential is different from the potential calculated by GYRO. In particular, in our model, the part of the potential that is outside the interval of the extended angle $\theta \in [-\pi, \pi]$ is neglected. This assumption gives reasonable results for the particle flux and the ion heat flux, but not for the electron heat flux, where the contribution of the part outside of $[-\pi, \pi]$ can be large. However, the nonlinear GYRO results show that the collisionality dependence of the electron heat flux is in fact almost negligible, therefore COMET gives qualitatively correct scaling with the collisionality in spite of the fact that it is unable to reproduce the collisionality dependence of the quasilinear GYRO results for the electron heat flux, due to the simplicity of the assumed ballooning potential.

C. Shear scaling

The validity of the model depends on the assumed electrostatic potential, the form of which is dependent on the shear. Some of the shear dependence is kept by using a shear-dependent factor f_s multiplying the imaginary part of the potential, but the width of the real part of the potential is not varied and the dependence of f_s on plasma parameters other than shear is neglected. Therefore the model is still too crude to capture all of the shear dependence of the problem. However, as illustrated in Fig. 6, where the shear dependence of the eigenvalues and fluxes are shown in the collisionless case, in the moderate shear region, the COMET results have reasonable agreement with quasilinear GYRO results.

V. CONCLUSIONS

In this paper we presented a semianalytical collisional model for electrostatic microinstabilities and the quasilinear transport fluxes driven by them. By assuming a ballooning eigenfunction for the electrostatic potential we obtained closed analytical expressions for the perturbed electron/ion density and temperature responses. The expressions contain

explicitly the dependence on electron-ion collision frequencies and no expansion in the smallness of ω_{Da}/ω is used. The collisions are modeled by the Lorentz operator, which gives the proper boundary layer development of the nonadiabatic trapped electron distribution at the trapped-passing boundary as it is shown in Ref. 11. We illustrated that the linear approximation of the hypergeometric functions, the so-called nonresonant expansion, is valid only in a very small vicinity of $\omega_{Da}/\omega=0$. Therefore it is not appropriate for typical ITG frequencies and it gives incorrect results for the parameter region we studied, where the density profile is not too steep. We introduced a simple algebraic approximation of these functions for $\omega_{Da}/\omega=\mathcal{O}(1)$ arguments.

Our model is semianalytical in the sense that the roots of the dispersion relation are obtained numerically. However, we found an exact ITG stability boundary in Eq. (24) for the $\epsilon\to 0$ and $\omega_{bi}/\omega\to 0$ limits, which incorporates not only the L_n/R and T_e/T_i, but also the shear and the FLR-parameter dependences. This stability boundary agrees well with numerical results obtained in GYRO. It has been shown that for a constant density gradient, increasing collisionality leads to a larger a/L_{Ti} threshold for stability. This means that decreasing collisionality gives rise to a destabilization of ITG mode driven turbulence, which in turn may lead to a steepening of the density profile.

We benchmarked our model to the recognized, state-of-the-art gyrokinetic simulation code GYRO and illustrated the agreement on the GA standard case.[5] The results for the eigenfrequencies and growth rates agree well with quasilinear gyrokinetic calculations with GYRO. Our results show that the toroidal ITG frequencies can be calculated accurately neglecting the parallel ion dynamics using a model ballooning potential. However it is important to take the shear dependent imaginary part of the potential into account. We motivated the model potential by a self-consistent variational solution of the ballooning eigenfunction problem.

The frequencies and growth rates of the ITG modes far from threshold are not very sensitive to the collisionality, but the quasilinear particle flux changes dramatically for very small collisionalities, in agreement with the results of Ref. 11 and of previously published gyrokinetic simulations, e.g., in Ref. 12. Expressions for the electron and ion particle and energy fluxes have been derived and from comparisons with quasilinear and nonlinear GYRO simulations we concluded that the COMET flux captures the qualitative collisionality dependence and a/L_{Ti}-scalings. The quantitative agreement between COMET and GYRO becomes worse for low and large shears, because the assumed form for the electrostatic potential is not a good approximation in that region. Reliable quantitative predictions for the eigenvalues and fluxes can therefore only be obtained in the moderate shear region.

ACKNOWLEDGMENTS

This work was funded by the European Communities under Association Contract between EURATOM and *Vetenskapsrådet*. The views and opinions expressed herein do not necessarily reflect those of the European Commission. The authors would like to thank P. Helander and H. Nordman for useful discussions of the paper.

APPENDIX A: MODEL FOR THE PERTURBED ELECTROSTATIC POTENTIAL

In order to motivate the chosen model for the perturbed electrostatic potential, it is convenient to follow a variational approach using a trial function for the perturbed electrostatic potential motivated by GYRO simulations:

$$\phi(\theta)=\phi_0[1+A\cos\theta+B\sin^2\theta+(1-A)\cos 3\theta]\times[H(\theta+\pi)-H(\theta-\pi)]. \tag{A1}$$

The coefficients A and B are determined by taking $\{1,\cos\theta,\sin^2\theta\}$ moments of the integrodifferential equation derived from the quasineutrality condition. A similar method was used by Ref. 19, where a trapped particle instability was considered. The potential was expanded in series in $\cos\theta$ and the coefficients were determined by taking moments of the equation resulting from the quasineutrality condition. More recent attempts to obtain a model electrostatic potential (see, e.g., Ref. 14) neglected the effect of the trapped particles, motivated by the smallness of the inverse aspect ratio. The neglect of the trapped population simplifies the mathematical problem considerably, since it removes the integral part of the equation. In reality the factor $\sqrt{2\epsilon}$ is not very small and the trapped population may have influence on the form of the potential. With the variational method outlined by Ref. 19, the effect of the trapped particle population can be kept, along with the terms resulting from the ion parallel motion. Unfortunately a full *analytical* solution of the problem is difficult, unless we neglect collisions and expand in the smallness of $v_{Ti}/\omega qR$, the FLR parameter b and normalized magnetic drift frequency ω_D/ω. Although these approximations restrict the validity of the model, it is still instructive to study what determines the shape of the ballooning potential.

We begin with a simplified version of the problem, by neglecting the ω_D-resonance, ion parallel motion and collisions. Then, the ion response can be obtained by neglecting the term proportional to ω_{D_s} in Eq. (16) and is

$$\frac{\hat{n}_i}{en_e/T_e}=-\{\tau\tilde{\omega}_{*i}+\tau b_s[1-\tilde{\omega}_{*i}(1+\eta_i)]\}\phi, \tag{A2}$$

where $b_s=b_0(1+s^2\theta^2)$ and the tilde denotes normalization with respect to ω. Neglecting collisions, the electron response can be obtained directly from Eq. (4),

$$\frac{\hat{n}_e}{en_e/T_e}=\phi-(1-\tilde{\omega}_{*e})\frac{1}{2}\int\frac{Bd\lambda}{\sqrt{1-\lambda B}}\langle\phi\rangle, \tag{A3}$$

where $\langle\cdots\rangle$ is an average over the bounce-orbit of the trapped electrons and the λ-integral is over the trapped electron population. Using Eqs. (A2) and (A3) the quasineutrality condition becomes

$$0=\frac{\hat{n}_e-\hat{n}_i}{en_e(1-\tilde{\omega}_{*e})}$$
$$=\frac{1+\tau\tilde{\omega}_{*i}+\tau b_s[1-\tilde{\omega}_{*i}(1+\eta_i)]}{1-\tilde{\omega}_{*e}}\phi-\frac{1}{2}\int\frac{Bd\lambda}{\sqrt{1-\lambda B}}\langle\phi\rangle, \tag{A4}$$

and it can be written as an integral equation

$$[q_0+(q_0-1)s^2\theta^2]\phi-\frac{1}{2}\int\frac{Bd\lambda}{\sqrt{1-\lambda B}}\langle\phi\rangle=0, \tag{A5}$$

where

$$q_0=\frac{1+\tau\tilde{\omega}_{*i}+\tau b_0[1-\tilde{\omega}_{*i}(1+\eta_i)]}{1-\tilde{\omega}_{*e}}. \tag{A6}$$

For the electrostatic potential we assume the trial function given in Eq. (A1) and take moments of the quasineutrality equation,

$$\frac{1}{2\pi}\int_{-\pi}^{\pi}d\theta\frac{\hat{n}_e-\hat{n}_i}{en_e(1-\tilde{\omega}_{*e})/T_e}\begin{bmatrix}1\\ \cos\theta\\ \sin^2\theta\end{bmatrix}=0, \tag{A7}$$

to obtain three equations that determine the coefficients of the perturbed potential A, B, and the eigenvalue q_0 that gives the dispersion relation.

For the parameters used throughout this paper ($\tau=1$, $\eta_i=\eta_e=3$, $\epsilon=1/6$, $s=1$, $q=2$, and $L_n/R=1/3$), the above simplified approach gives the eigenvalue $q_0=0.46$ and the coefficients for the eigenfunction: $A=0.75$ and $B=-1.3$. The real part of the potential is similar to the one obtained by GYRO, but due to the neglect of the parallel ion motion and ω_D resonance, the information about the imaginary part of the potential is lost. Note that for the simple ion response given in Eq. (A2) the parameters A, B, and q_0 can be calculated without any assumption on the mode frequency.

Including parallel ion motion and the effect of the ω_{Di} resonance to leading order, the ion response is given by

$$\frac{\hat{n}_i}{en_e/T_e}=\phi\tau\Bigg(-\tilde{\omega}_{*i}-b_0[1-\tilde{\omega}_{*i}(1+\eta_i)]+\frac{q_0-1}{b_0}(1-\tilde{\omega}_{*e})\Bigg\{-b_0s^2\theta^2+\frac{3\tilde{\omega}_{Di}}{2}+\delta^2\frac{\phi''}{\phi}\left[\frac{5b_0}{6}-\frac{1}{2}+\frac{5}{3}\left(\frac{b_0s^2\theta^2}{2}-\frac{15\tilde{\omega}_{Di}}{4}\right)\right]\Bigg\}\Bigg), \tag{A8}$$

where the term proportional to $\delta^2=v_{Ti}^2/\omega^2q^2R^2$ represents the contribution from the parallel ion motion and we used the CER approximation. Neglecting electron-ion collisions and the ω_{De} resonance the electron response is given by Eq. (A3).

The shape of the ballooning potential and the mode frequency ω can be self-consistently calculated using the following iteration scheme. By the solution of the three coupled equations resulting from the integrals given in Eq. (A5), the parameters A, B, and q_0 can be determined for a given ω. A new ω can be obtained from the solution of Eq. (A4), which is fed back to the previous system of equations. For our standard parameters it leads to the eigenvalue: $q_0=0.99-0.11i$, mode frequency $\omega=\omega_{*e}(-1.0+2.3i)$, and the coefficients for the perturbed potential are $A=1.1+0.060i$ and $B=0.049+0.59i$. The potential corresponding to these values is plotted in Fig. 1 with green dashed line, together with the one computed by GYRO with and without ion parallel motion, and the one we use in the paper. The potential calculated in this way agrees very well with the result of the GYRO simulation. We note that taking into account the effect of the ω_D-resonance to first order and parallel ion motion is important to obtain the correct sign of the factor multiplying the imaginary part of the potential.

TABLE I. Coefficients in the approximative formulas.

	$\mathcal{F}^1_{5/2}$	$\mathcal{F}^1_{7/2}$	$\mathcal{F}^1_{9/2}$	$\mathcal{F}^{3/2}_{3/4}$	$\mathcal{F}^{3/2}_{7/4}$	$\mathcal{F}^{3/2}_{11/4}$
c	2.12	2.56	2.89	1.21	2.35	3.17
$c\approx$	2	5/2	3	5/4	5/2	3

APPENDIX B: APPROXIMATION OF THE HYPERGEOMETRIC FUNCTIONS IN THE RELEVANT PARAMETER REGIME

Since the frequency of the toroidal ITG mode is typically of the order of the magnetic drift frequency, the nonresonant expansion, i.e., the expansion in the smallness of ω_{Da}/ω, is not appropriate, as it is illustrated on Fig. 2. In order to obtain simple algebraic expressions for the perturbed density and temperature responses [given in Eqs. (9), (13), (11), and (14), respectively] we introduce approximations for the generalized hypergeometric functions $\mathcal{F}^{a_2}_{a_1}(z)$ appearing in these expressions. These approximations are valid for $|z|=\mathcal{O}(1)$ arguments and exact in the $z\to0$ limit. In our analysis, we assumed that $\omega_{bi}\ll\omega$, which gives an upper limit for the argument of the hypergeometric functions, namely, $z\sim\omega_{Da}/\omega$ cannot be much higher than one. Therefore we do not needed the approximation to be valid asymptotically as $z\to\infty$.

For arguments that are not too large ($|z|<3$), we can approximate the generalized hypergeometric function $\mathcal{F}^{a_2}_{a_1}(z)={}_2F_0(a_1,a_2;;z)$ by

$$\mathcal{F}^{a_1}_{a_2}(z)\approx(1-\sqrt{b}+\sqrt{b-z})^{-c}, \tag{B1}$$

where $b=c^2/(4a_1a_2)$ and c is a constant that can be found by the minimization of the absolute value of the integral difference between the exact and approximate functions for a finite radius domain of the complex plane. The constant is not a low order rational number in general, but can be approximated with a properly chosen one, still providing a very good approximation for $\mathcal{F}^{a_2}_{a_1}$. The values of c corresponding to the best approximation in the above sense for $|z|<3$ and their rational approximations are listed in Table I. The average integral difference of the approximative algebraic expression and the exact hypergeometric function on the $|z|<3$ domain was shown to be below 4% if the constant c is chosen to be a rational number. In Figs. 4–6 the eigenvalues and

fluxes calculated using the approximative formula (B1) with the rational approximations of c are shown with purple dotted lines. The eigenvalues and fluxes calculated with the approximation in Eq. (B1) are in excellent agreement with the ones calculated with the exact hypergeometric functions.

[1] J. W. Connor and H. R. Wilson, Plasma Phys. Controlled Fusion **36**, 719 (1994).
[2] W. Horton, Rev. Mod. Phys. **71**, 735 (1999).
[3] X. Garbet, P. Mantica, C. Angioni, E. Asp, Y. Baranov, C. Bourdelle, R. Budny, F. Crisanti, G. Cordey, L. Garzotti, N. Kirneva, D. Hogeweij, T. Hoang, F. Imbeaux, E. Joffrin, X. Litaudon, A. Manini, D. C. McDonald, H. Nordman, V. Parail, A. Peeters, F. Ryter, C. Sozzi, M. Valovic, T. Tala, A. Thyagaraja, I. Voitsekhovitch, J. Weiland, H. Weisen, A. Zabolotsky, and the JET EFDA Contributors, Plasma Phys. Controlled Fusion **46**, B557 (2004).
[4] J. Weiland, *Collective Modes in Inhomogeneous Plasma* (Institute of Physics, Bristol, 2000).
[5] J. Candy and R. E. Waltz, J. Comput. Phys. **186**, 545 (2003).
[6] C. Angioni, A. G. Peeters, G. V. Pereverzev, F. Ryter, G. Tardini, and the ASDEX Upgrade Team, Phys. Rev. Lett. **90**, 205003 (2003).
[7] C. Angioni, A. G. Peeters, G. V. Pereverzev, F. Ryter, and G. Tardini, Phys. Plasmas **10**, 3225 (2003).
[8] H. Weisen, A. Zabolotsky, C. Angioni, I. Furno, X. Garbet, C. Giroud, H. Leggate, P. Mantica, D. Mazon, J. Weiland, L. Zabeo, K.-D. Zastrow, and the JET-EFDA Contributors, Nucl. Fusion **45**, L1 (2005).
[9] M. Greenwald, C. Angioni, J. W. Hughes, J. Terry, and H. Weisen, Nucl. Fusion **47**, L26 (2007).
[10] H. Takenaga, K. Tanaka, K. Muraoka, H. Urano, N. Oyama, Y. Kamada, M. Yokoyama, H. Yamada, T. Tokuzawa, and I. Yamada, Nucl. Fusion **48**, 075004 (2008).
[11] T. Fülöp, I. Pusztai, and P. Helander, Phys. Plasmas **15**, 072308 (2008).
[12] C. Estrada-Mila, J. Candy, and R. E. Waltz, Phys. Plasmas **12**, 022305 (2005).
[13] F. Romanelli and S. Briguglio, Phys. Fluids B **2**, 754 (1990).
[14] F. Romanelli, L. Chen, and S. Briguglio, Phys. Fluids B **3**, 2496 (1991).
[15] S. C. Guo and F. Romanelli, Phys. Fluids B **5**, 520 (1993).
[16] M. A. Beer and G. W. Hammett, Phys. Plasmas **3**, 4018 (1996).
[17] J. W. Connor, R. J. Hastie, and P. Helander, Plasma Phys. Controlled Fusion **48**, 885 (2006).
[18] I. S. Gradshteyn and I. M. Ryzhik, *Table of Integrals, Series, and Products*, 7th ed. (Academic, New York, 2007).
[19] B. B. Kadomtsev and O. P. Pogutse, Rev. Plasma Phys. **5**, 249 (1970).